ORIGINAL PAPER

Biologically Inspired Dynamic Soaring Maneuvers for an Unmanned Air Vehicle Capable of Sweep Morphing

Imran Mir[1] · Adnan Maqsood[1] · Suhail Akhtar[2]

Abstract

Dynamic soaring is a versatile maneuver executed to acquire energy available in the atmospheric wind shears. In this paper, an innovative concept of integrating wing sweep morphing during dynamic soaring maneuver is proposed. An unmanned air vehicle (UAV) with standard wing–tail configuration is considered. The aerodynamic modeling is based on the empirical estimation procedure duly validated with numerical vortex lattice method (VLM). The dynamics of the UAV is modeled as a three-dimensional point-mass model with nonlinear wind shear. The trajectory optimization problem is formulated as an optimal control problem using Guass pseudospectral method. The comparison of wing sweep morphing ability during flight is compared with its fixed-wing counterpart. Typical performance parameters used for comparison between both configurations include minimum wind shear and aerodynamic efficiency. Results indicate significant reduction in the minimum wind shear requirement (24%) and considerable improvement in the aerodynamic efficiency (24% drag reduction, 10% less lift coefficient requirement, 34% higher normalized energy and 25% improved loitering performance). A great potential of further exploring and coupling different wing-morphing mechanisms to further extract potential benefits of dynamic soaring maneuvers is proposed. This investigation will serve as a baseline for the proof of concept that dynamic soaring can be extended to a morphing platform in achieving optimal performance.

Keywords Dynamic soaring · Trajectory optimization · Morphing · Nonlinear simulation

1 Introduction

The operational deployment of small unmanned air vehicles (sUAVs) is always challenging due to their endurance and range limitations. Efforts in the form of enhancing aerodynamic efficiency, swarming technology and battery performance improvement through solar or fuel cells are typically adopted. Another emerging area to improve range and endurance of these platforms is the usage of biologically inspired aerodynamic maneuvers (Fig. 1),which are classified into two broad categories. The first one does not cater for atmospheric wind shears and can be executed anywhere. These include transitions between hover and cruise [1,2],

perching [3–5] and in-flight morphing [6,7] strategies. The second class is primarily dependent on soaring strategies [8–10]. The soaring maneuvers belong to the domain of active maneuvers, as they are dependent on atmospheric currents and wind shears. Among soaring, dynamic soaring [11] is of profound importance, as it enables UAV to perform powerless flight by actively acquiring energy available in atmospheric vertical wind gradients. It is potentially of greater utility than static and gust soaring, as the wind gradients are more predictable and are present whenever there is wind. Additionally, it is robust with respect to weather and its primary advantage is in picking up speed, in contrast to static soaring, which is mere harnessing of lift.

The seminal work on dynamic soaring can be traced back to Lord Rayleigh in 1883 [12]. Subsequent research for decades focused on understanding the basics of flight of soaring birds. This understanding improved drastically with the emergence of digital technology. Alberstam [13] and Weimerskirch [14] tracked albatross by satellite and other measurement devices and reported useful information in ascertaining the flight performance parameters of soaring

✉ Imran Mir
  imranmir56@yahoo.com

[1] Research Center for Modeling and Simulation, National University of Sciences and Technology (NUST), Islamabad, Pakistan

[2] College of Aeronautical Engineering, National University of Sciences and Technology (NUST), Islamabad, Pakistan
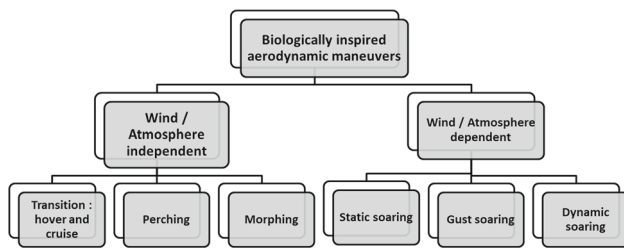
Fig. 1 Broad classification of biologically inspired maneuvers

flight. Since dynamic soaring is dependent upon wind shear, geographical regions in which sufficient wind shear exists to facilitate dynamic soaring were also identified [15,16]. Data given by Idrac [17] and Sachs [18] refer to a wind speed of 5 m/s close to the sea surface as the lowest permissible value for dynamic soaring. For full-scale aircraft, Sachs and Da Costa [16] showed that dynamic soaring by full-size sailplanes is possible with values of wind shear found near mountain ridges. Gordan [19] carried out a detailed search on extending dynamic soaring to full-sized planes and ascertained that full-size sailplanes could extract energy from horizontal wind shears, although the utility of the energy extraction could be marginal depending on the flight conditions and the type of sailplane used. Zhao [20] analyzed different optimal dynamic soaring patterns (loiter, travel and basic modes) of a glider by incorporating optimal control techniques and effects of wind gradient slope and profile nonlinearity. Zhao and Qi [21] examined minimum fuel-powered dynamic soaring of UAV (both propeller-driven and jet-driven) assuming a linear wind gradient profile and a three-dimensional point-mass UAV model.

In all cases, however, the base line model utilized for dynamic soaring have always been a fixed configuration [10,11,22–25] in which the platform cannot change its configuration. However, soaring birds such as albatross, can morph their wings during different phases of flight to enhance their maneuver potential [26]. They can effectively vary wing sweep, wing span, wing twist, wing dihedral as well as wing anhedral with the shoulder lock fixed-wing flying [9,27]. As soaring birds while performing dynamic soaring acquires optimum energy from atmosphere under morphing condition, a biologically inspired morphable platform with the ability to vary its planform parameters is envisaged to efficiently optimize the energy gain from the atmosphere.

Morphing has a significant impact on aerodynamic characteristics of the flying vehicle and remarkable improvement in the flight regime is achieved by employing different morphing techniques [28,29]. Although there is a lot of versatility in morphing schemes, such as wing [30], fuselage [31], tail [32] or engine [33] morphing, altering wing parameters (such as wing planform, airfoil shape and so on) have the most powerful and influential impact on the performance parameters

[34]. For span variation, inflatable telescopic wing design is normally a preferred choice as it has the ability to undergo a 114% change [35] in aspect ratio while supporting aerodynamic loads. Similarly, increase/ decrease in sweep angles [36] causes corresponding changes in parameters such as critical mach number, dihedral effect, high-speed drag and maximum lift coefficient $C_{L_{max}}$. Wings with higher sweep angle are more advantageous in attaining the highest maximum speed (dash), while the smaller wing sweep angle is more suitable for higher range and endurance for loiter / reconnaissance missions. Similarly, wing dihedral [37] variation affects rolling moment $C_{l_{max}}$ and lateral stability. Amongst these available morphing techniques, the technique most suitable for dynamic soaring is therefore to be identified for ascertaining the platform configurations during different phases of the maneuver.

As demonstrated by soaring birds, different planform configurations are required during the dynamic soaring maneuver to ensure maximum energy extract from the atmospheric wind shear [27]. It is ,however, noticeable that a planform configuration suitable for achieving desired performance during a particular stage of the maneuver may adversely effect the performance parameters in the other phase [38]. As an example, for enhanced forward length distance of the energy neutral dynamic soaring cycle, wings with lower span, higher sweep and dihedral configurations are preferred for speedy climb with higher velocity and more rolling stability [28,39]. However, wings with extended span and minimum sweep angle are desired during the descent phase to achieve higher cruise distance [26,40]. Also, high directional stability is required during climb and descent phases of the soaring flight to avoid unnecessary control effort [41,42]. However, the same is not desirable during high and low altitude turn phases of the maneuver [43,44], as considerably large control effort will be required to overcome this directional stability.

In this research, the impact of sweep variation on dynamic soaring is investigated. Detailed analysis for integrating dynamic soaring trajectories under morphing conditions is performed for a UAV capable of performing sweep variations. After selecting a generic UAV platform, its aerodynamic model is generated through empirical formulas readily available in literature. The trajectory generation problem is modeled as a nonlinear-constrained optimization problem with objective function, constraints on aircraft states and controls, and point-mass dynamic model with nonlinear wind shear model [11,20,21]. The algorithm used for trajectory optimization is based on Guass pseudospectral technique, commercially available as GPOPS-II [45]. In results and discussion section, comparison of advantages between fixed and sweep capable configuration is made. Comparisons are made in the form of state and control variables and performance parameters that include cycle time, maximum achievable velocity, minimum required wind shear, maximum altitude
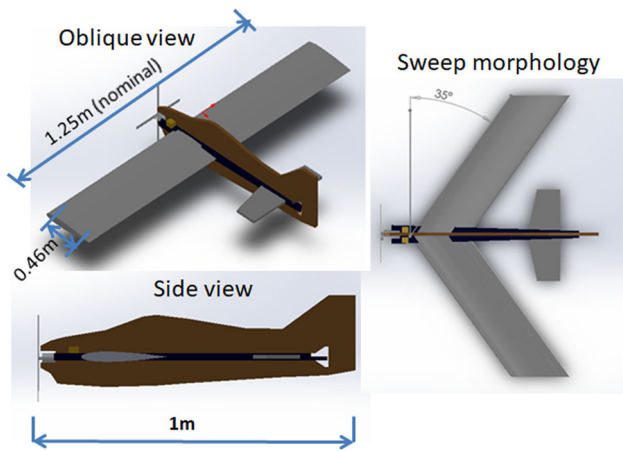
Fig. 2 Oblique and side views of the morphing UAV considered in this study

gain, distances covered in the east/north direction, aerodynamic forces and so on.

2 Problem Setup

2.1 Aircraft Model Description

The aircraft model considered consists of a conventional radio controlled (RC) standard wing–tail configuration as shown in Fig. 2. The dimensions of the aircraft include fuselage length of 1 m, wing span of 1.5 m, mean aerodynamic chord of 0.4640 m, aspect ratio of 3.232, nominal wing sweep of $0°$, wing area of $0.696 \, \text{m}^2$, taper ratio of 1 and aerodynamic surfaces are constructed from NACA 0012 airfoil. The recommended all up weight (AUW) for enhanced performance is about 1.6 kg. The wing is assumed to have an internal mechanism with sweep capability up to $50°$.

The moment of inertias are calculated by assuming body to be rigid at a particular orientation. The symmetrical inertia tensor at $0°$ sweep angle and origin at centre of gravity is defined in Eq. (1)

$$\boldsymbol{I} = \begin{bmatrix} I_{xx} & -I_{xy} & -I_{xz} \\ -I_{xy} & I_{yy} & -I_{yz} \\ -I_{xz} & -I_{yz} & I_{zz} \end{bmatrix}$$

$$= \begin{bmatrix} 5377694.89 & -3859.41 & -6807.93 \\ -3859.41 & 24885559.95 & -3209.00 \\ -6807.93 & -3209.00 & 23093644.43 \end{bmatrix} \text{g mm}^2.$$

$$(1)$$

2.2 Nonlinear flight dynamic modeling

The equations of motion considered to model the flight dynamics of the aircraft are coupled and nonlinear in nature. It is assumed that the three-dimensional point-mass model
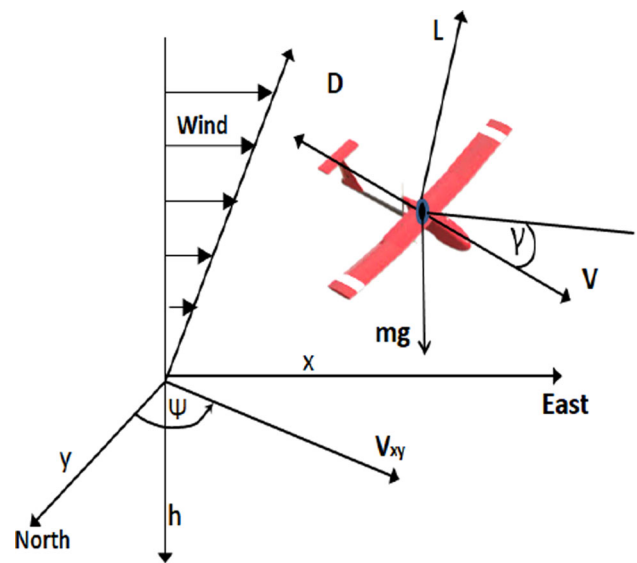

Fig. 3 UAV orientation during the dynamic soaring maneuver

considered in the study will represent the qualitative behavior of the aircraft dynamics and elaborate model may not be required to assess the macro level contribution of sweep effect on dynamic soaring trajectories. The dynamic modeling utilized in this study is aligned with other studies [20,21,46] for describing system dynamics and elaborated in Eq. (2)

$$\dot{V} = \frac{1}{m}[-D - mg \sin \gamma - m\dot{V}_W \cos \gamma \sin \psi]$$

$$\dot{\psi} = \frac{1}{mV_t \cos \gamma}[L \sin \phi - m\dot{V}_W \cos \psi]$$

$$\dot{\gamma} = \frac{1}{mV_t}[L \cos \phi - mg \cos \gamma + m\dot{V}_W \sin \psi \sin \gamma] \qquad (2)$$

$$\dot{x} = V \cos \gamma \sin \psi + V_W$$

$$\dot{y} = V \cos \gamma \cos \psi$$

$$\dot{h} = V \sin \gamma$$

where V is the UAV velocity, V_W is the wind velocity, γ is the flight path angle, ψ is the heading angle, ϕ is the bank angle, L is the lift, D is drag, m is the mass of the UAV, and x, y, h are the position vectors in the direction of inertial north, east, and down, respectively. In this model, the speed of UAV is modeled in a wind relative reference frame and the position of UAV is modeled in an earth-fixed frame (North, east, down) as shown in Fig. 3

Typically, wind shear estimation during dynamic soaring maneuver is done either through some known model once the wind conditions are known or online estimation of wind shear in unknown wind conditions. In this study, the wind shear velocity V_W is approximated with well-established nonlinear logarithmic wind shear model [11,18] model. The logarithmic relation between wind velocity (V_W) and height above the surface (h) is given by Eq. (3)

$$V_W = V_{w_{\text{ref}}} \frac{\ln(h/h_0)}{\ln(h_{\text{ref}}/h_0)}, \tag{3}$$

where $V_{w_{\text{ref}}}$ represents the strength of the wind shear velocity at reference altitude h_{ref}. Also, h_0 is the surface correctness factor that determines the distribution of the wind gradient with varying altitude, reflecting the surface properties, such as irregularity, roughness and drag. The values $h_{\text{ref}} = 10$ m and $h_0 = 0.03$ m are chosen in this study [18]. The minimum reference wind speed value at this altitude, which still permits dynamic soaring is ascertained through the optimization process.

The wind shear gradient is represented by Eq. (4):

$$\dot{V}_W = V_{w_{\text{ref}}} \frac{1}{h \ln(h_{\text{ref}}/h_0)} \dot{h}, \tag{4}$$

where $\dot{h}$ is the rate of change in the altitude.

The lift and drag forces acting on the UAV vary with varying sweep angle and angle of attack through the following empirical relation

$$L = 0.5\rho V^2 S C_L \quad \text{and} \quad D = 0.5\rho V^2 S C_D \tag{5}$$

where ρ is the density of the air and S is the wing area. The lift and drag are the functions of the angle of attack and sweep angle and are determined through empirical techniques. The lift coefficient is determined using the relationship

$$C_L = C_{L_\alpha}(\alpha - \alpha_{L=0}) \tag{6}$$

where C_{L_α} is the lift curve slope of the wing, α is the angle of attack and $\alpha_{L=0}$ is the angle of attack at zero lift. The lift curve slope of the wing is determined utilizing the empirical relationship [47]

$$C_{L_\alpha} = \frac{c_{L_\alpha} \cos \Lambda}{\sqrt{(1 + c_{L_\alpha} K \cos \Lambda)^2} + c_{l_\alpha} K \cos \Lambda} \tag{7}$$

where c_{L_α} is the lift curve slope of the cross-section. The induced drag factor (K) is defined as

$$K = \frac{1}{\pi e \text{AR}} \tag{8}$$

where e is the span efficiency factor having a value of 0.8. Also, AR is the wing aspect ratio and is calculated using the relationship

$$\text{AR} = b_{\text{eff}}^2 / S_{\text{eff}} \tag{9}$$

where b_{eff} is the effective wing span and S_{eff} is the effective wing area. The effective wing span and the effective wing area (in case of leading edge sweep) are related to the nominal
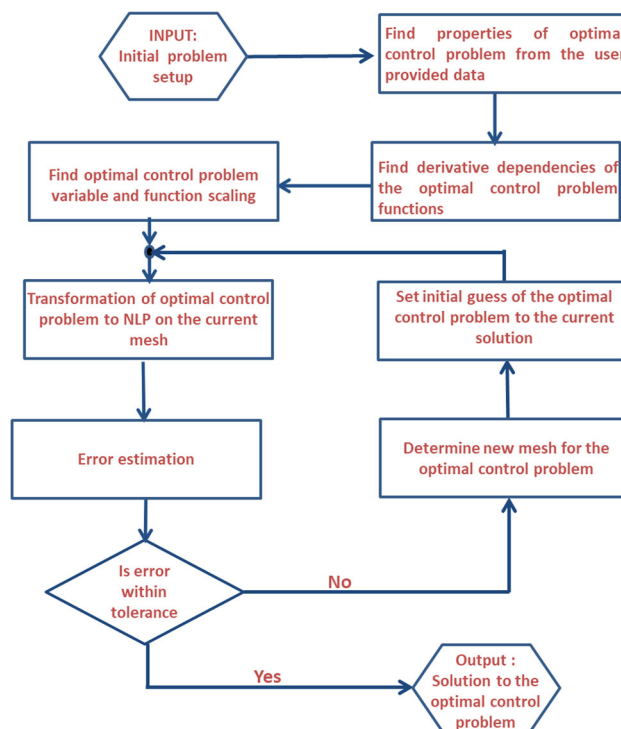

Fig. 4 Operational flow chart of GPOPS– II [45]

wing span b_{nom} and nominal area S_{nom} through sweep angle. This is governed by Eq. (10)

$$b_{\text{eff}} = b_{\text{nom}} \cos \Lambda, \quad S_{\text{eff}} = S_{\text{nom}} - \Delta S \tag{10}$$

where ΔS is the change in wing area due to sweep variation and is given as

$$\Delta S = 0.5 c_{\text{nom}}^2 \tan \Lambda \tag{11}$$

where c_{nom} is the nominal wing chord. The parabolic drag coefficient is given by Eq. (12)

$$C_D = C_{D_0} + K C_L^2 \tag{12}$$

where C_{D_0} is the zero lift drag coefficient.

2.3 Trajectory Optimization Setup

The optimal optimization evaluation is done using a commercially available algorithm GPOPS-II [45] integrated with MATLAB®. The algorithm is based on state-of-the-art hp-adaptive version of the Legendre–Gauss–Radau (LGR) orthogonal collocation method. This algorithm has been rigorously tested in different studies [24,48–53]. The operational functionality [45] of the GPOPS-II is demonstrated in Fig. 4. The flow chart explains the intermediate steps adopted in the algorithm starting from the user-provided input data

Table 1 Path constraints and numeric bounds for implementing loiter maneuver

No	Minimum value	Parameter	Maximum value	Numeric values
1	$x_{\min}$	x	$x_{\max}$	$x_{\min} = -200$ m, $x_{\max} = 200$ m
2	$y_{\min}$	y	$y_{\max}$	$y_{\min} = -200$ m, $y_{\max} = 200$ m
3	$z_{\min}$	z	$z_{\max}$	$z_{\min} = 0$, $z_{\max} = 100$ m
4	$V_{\min}$	V	$V_{\max}$	$V_{\min} = 3$ m/s, $V_{\max} = 30$ m/s
5	$\gamma_{\min}$	γ	$\gamma_{\max}$	$\gamma_{\min} = -70°$, $\gamma_{\max} = 70°$
6	$\psi_{\min}$	ψ	$\psi_{\max}$	$\psi_{\min} = -400°$, $\psi_{\max} = 50°$
7	$\phi_{\min}$	ϕ	$\phi_{\max}$	$\phi_{\min} = -70°$, $\phi_{\max} = 70°$
8	$t_{cyc_{\min}}$	t_{cyc}	$t_{cyc_{\max}}$	$t_{cyc_{\min}} = 1$ s, $t_{cyc_{\max}} = 15$ s
9	$n_{\min}$	n	$n_{\max}$	$n_{\min} = 0$, $n_{\max} = 7$

for the optimal control problem to the computation of the optimal solution.

The flight model described by Eq. (2) with nonlinear wind profile Eq. (3) is configured as a nonlinear system of the form specified in Eq. (13):

$$\dot{x} = F(x(t), u(t)). \tag{13}$$

The flight dynamics model includes six states variables (which are function of a time period t), as defined in Eq. (14):

$$x(t) = [V, \ \psi \ \gamma, \ x, \ y, \ h]^T, \quad x(t) \in \mathbb{R}^6 \tag{14}$$

Control vector for fixed (non-morphing) configuration is defined in Eq. (15)

$$u(t) = [\alpha, \ \phi]^T, \quad u \in \mathbb{R}^2 \tag{15}$$

where ϕ is the bank angle.

Control vector $u(t)$ for sweep morphology is defined as

$$u(t) = [\Lambda, \ \alpha, \ \phi]^T, \quad u \in \mathbb{R}^3 \tag{16}$$

where Λ denotes the wing sweep angle.

Dynamic soaring flight is then formulated as a nonlinear optimal control problem to find a control $u(t)$ that optimizes performance function specified in Eq. (17) [9,23] subject to the dynamic constraints in Eqs. (2), and satisfying path and boundary constraints.

$$J = \min[V_{w,\mathrm{ref}}] \tag{17}$$

where $V_{w,\mathrm{ref}}$ (wind velocity at reference altitude) is the parameter to be minimized by the optimization algorithm. Different modes of dynamic soaring (basic, loiter, and forward flight modes) are implemented through boundary constraints [20]. Boundary conditions for implementing loiter mode of dynamic soaring is depicted at Eq. (18):

$$V_{t_f} = V_{t_0}, \psi_{t_f} = \psi_{t_0}, \gamma_{t_f} = \gamma_{t_0}, , x_{t_f} = x_{t_0},$$

$$y_{t_f} = y_{t_0}, h_{t_f} = h_{t_0}, \tag{18}$$

where V_{t_0}, ψ_{t_0}, γ_{t_0}, x_{t_0}, y_{t_0}, and h_{t_0} represents the state vector at initial time t_0 and V_{t_f}, ψ_{t_f}, γ_{t_f}, x_{t_f}, y_{t_f}, and h_{t_f} represents the state vector at final time t_f.

Path constraints and numerical bounds for the states and control during the dynamic soaring maneuver are depicted in Table 1. Since dynamic soaring is a high maneuvering cycle, which generates high accelerations, an additional path constraint of load factor (n) is included, which gives a global measure of the load to which the aircraft structure is subjected to.

In this problem, the initial orientation that is $[x, y, h]$ is kept constrained at $[x_0, y_0, h_0]$ (value within the permissible range depicted in Table 1). A value of $[x_0, y_0, h_0] = [0, 0, 0]$ was chosen as the initial point of the maneuver. The initial airspeed, flight path angle and heading angle $[V_{\mathrm{init}}, \gamma_{\mathrm{init}}, \psi_{\mathrm{init}}]$ are however left unconstrained (within the permissible range). This allows the optimization process to determine their optimal values for sustainable soaring flights.

3 Results and Discussion

This section deals with the quantification of benefits achieved through wing sweep morphing over fixed-wing configuration. To conduct intelligence, surveillance and reconnaisance (ISR) missions, UAVs are desired to loiter over a certain area for extended time periods. A representative case of the optimized dynamic soaring trajectories in loiter mode are compared in Fig. 5 under same atmospheric conditions. It can be seen that the morphing platform outperformed fixed configuration in terms of altitude gain and area coverage under similar wind shear and allied flight conditions. An approximate increase of 29%, 28% and 25% are observed in altitude gain, distance traveled along the east and north directions, respectively. By incorporating variable-sweep phenomena, aerodynamic advantages are harnessed
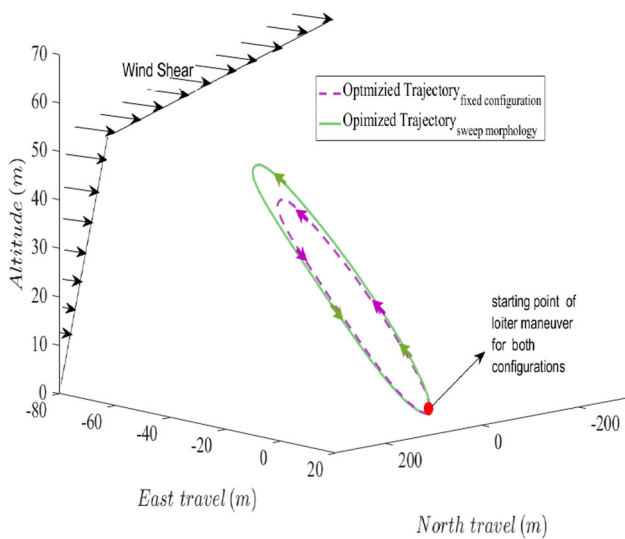
Fig. 5 UAV-optimized trajectories during the loiter maneuver

from the atmosphere thereby expanding the flight performance envelope of the dynamic soaring maneuver.

An elaborate analysis of the state histories for both morphing and fixed configurations is presented in Fig. 6. The velocity decreases during the windward climb phase of the maneuver and approaches zero at the highest point. Subse-

quently, the UAV picks up the speed after high altitude turn in which it experiences tailwind. The decrease in altitude results in converting potential energy to kinetic energy. Both UAVs start from the same point in the space. For variable-sweep case, an approximate increase of 13% in the maximum velocity attained during the maneuver is observed.

As shown in Eq. (2), to have powerless flight, the velocity added by wind shear (third term) must be greater than or at least even with that consumed by drag (first term).

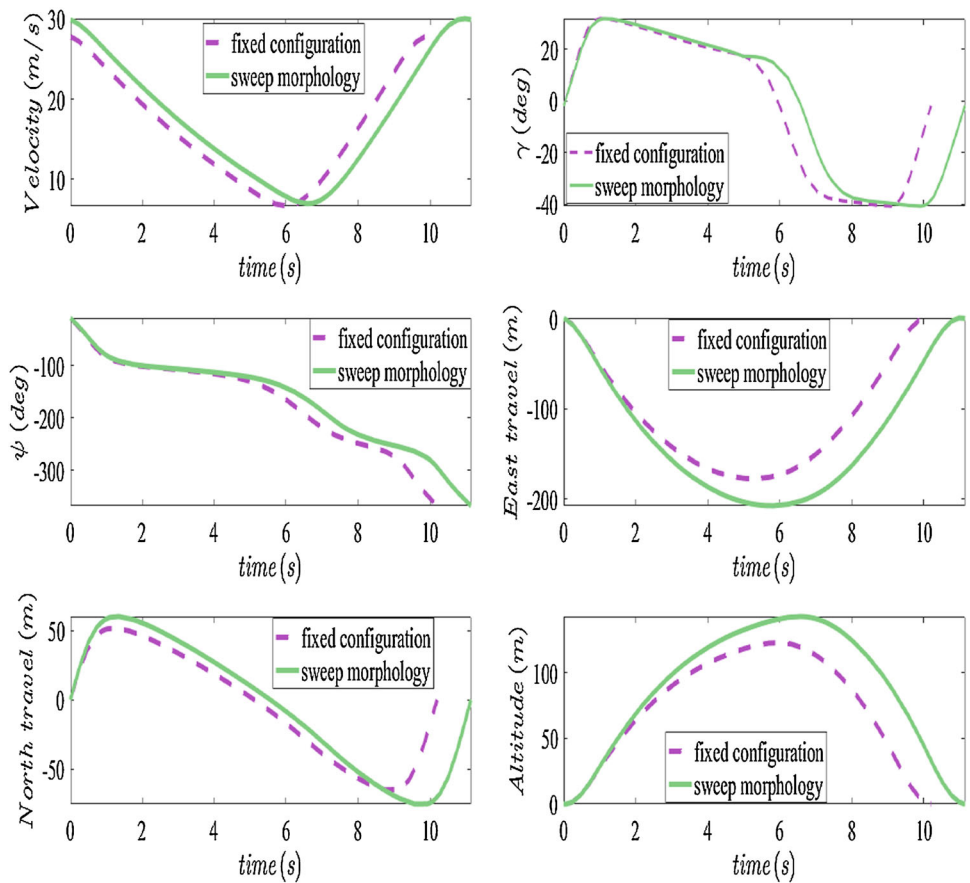$$\dot{V} = \frac{1}{m}[-D - mg \sin \gamma - m\dot{V}_W \cos \gamma \sin \psi] \tag{19}$$

From Eq. (4)

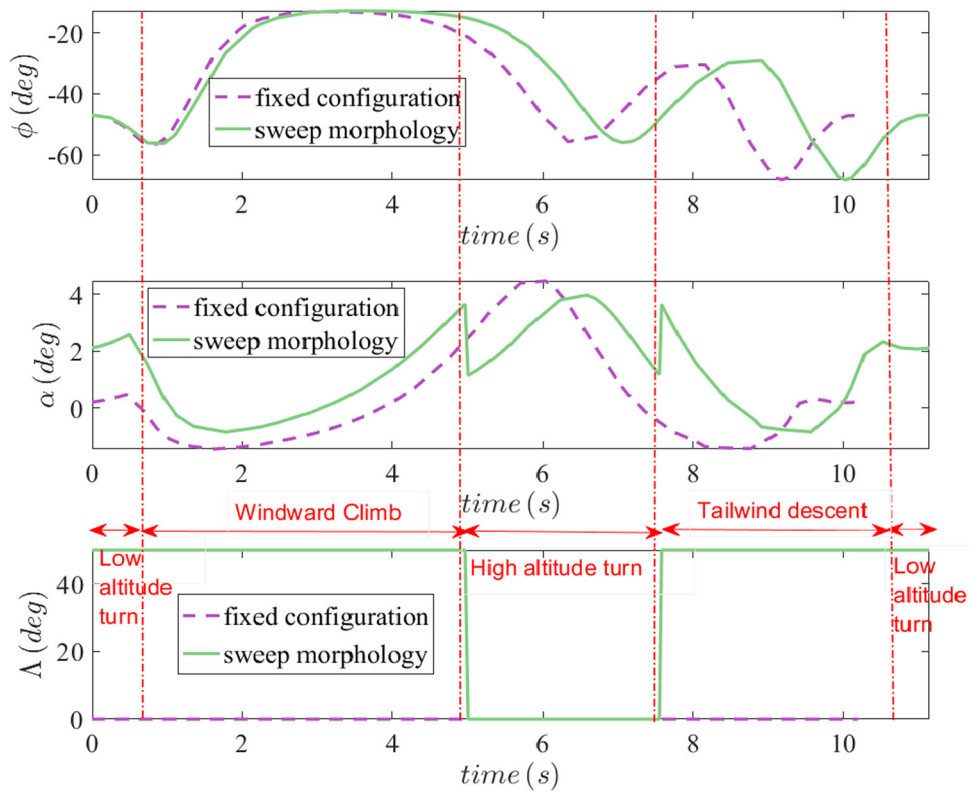$$\dot{V}_W = V_{w_{\mathrm{ref}}} \frac{1}{h \ln(h_{\mathrm{ref}}/h_0)} \dot{h}. \tag{20}$$

And from Eq. (2),

$$\dot{h} = V \sin \gamma. \tag{21}$$

Fig. 6 UAV states during the loiter maneuver

Fig. 7 UAV controls during four different phases of the loiter maneuver

So Eq. (19) transforms to Eq. (22):

$$
\dot{V} = \frac{1}{m}\left[-D - mg\sin\gamma \right.
$$
$$
\left. - mV_{w_{\mathrm{ref}}}\frac{1}{h\ln(h_{\mathrm{ref}}/h_0)}\sin\gamma\cos\gamma\sin\psi \right].
\tag{22}
$$

This requires that estimates (23) must be satisfied for sustained powerless flight.

$$
\sin\gamma\,\cos\gamma\,\sin\psi < 0. \tag{23}
$$

This can be achieved through windward climb and tailwind descend. During the windward climb phase, estimate (24) holds.

$$
\begin{aligned}
&0 < \gamma < \pi/2 \Rightarrow \sin\gamma\ \&\ \cos\gamma > 0,\\
&\pi < \psi < 2\pi\ \ \text{or}\ -\pi < \psi < 0, \Rightarrow \sin\psi < 0,\\
&\text{so overall,}\ \ \sin\gamma\,\cos\gamma\,\sin\psi < 0.
\end{aligned}
\tag{24}
$$

And during the decent phase, estimate (25) holds.

$$
\begin{aligned}
&-\pi/2 < \gamma < 0 \Rightarrow \sin\gamma < 0,\ \&\ \cos\gamma > 0,\\
&0 < \psi < \pi\ \ \text{or}\ -\pi < \psi < -2\pi, \Rightarrow \sin\psi > 0,\\
&\text{so overall,}\ \ \sin\gamma\,\cos\gamma\,\sin\psi < 0.
\end{aligned}
\tag{25}
$$

UAV can therefore extract energy from the atmosphere, during both the climb and descent phases. The optimized trajectories of flight path angle and heading angles (Fig. 6) reflects that the constraints imposed by estimate (24) and estimate (25) are completely satisfied.

The results can be further corroborated with the control vector history plotted in Fig. 7. The fixed configuration retains zero sweep during the complete maneuver. For morphing configuration, the wings sweep back to 50° during windward climb and tailwind descent phases. The associated angle of attack requirement is also less thereby suggesting towards low drag desirability during these phases. At higher altitude, drag penalty is finished due to reduced velocity. At this moment, the morphing wing goes to minimum sweep condition, that is 0°. In this phase, the aircraft wants to extract maximum lift from its aerodynamic surfaces. This suggest that the aircraft is trying to circumvent the stall conditions.

The UAV maintains the lower sweep configuration throughout the high altitude turn phase. During the tailwind descent, the wings sweep back to 50°, low drag configuration, after crossing the threshold velocity of 10.62 m/s (refer Fig. 8). Another important observation made from the state and control histories is increase in overall loiter time per cycle with morphing. This is also a desirable attribute in enhancing loiter performance. The algorithm performs rapid optimization of the sweep during various phases within the permissible range. In real-world conditions, a rate limiter can be incor-
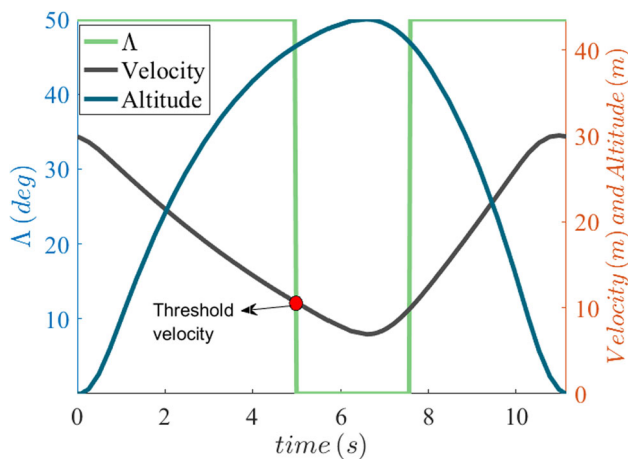
Fig. 8 Sweep variation during the loiter maneuver

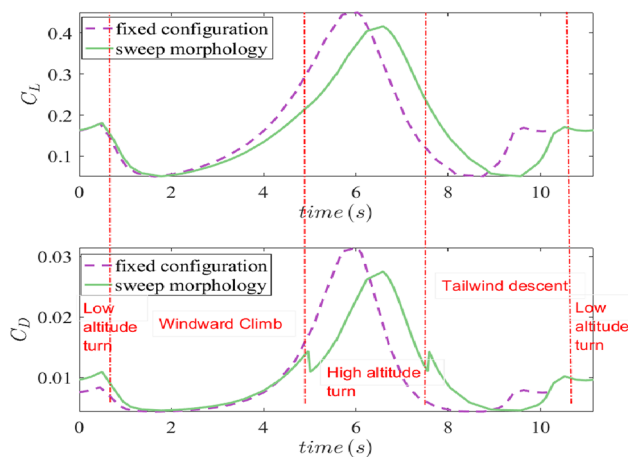Fig. 10 Aerodynamic coefficient comparison : empirical Vs VLM techniques

Fig. 9 Aerodynamic coefficients during four different phases of the loiter maneuver

porated to ensure that the change in the sweep variations is not beyond admissible rates for the wing actuators.

The history of aerodynamic coefficients is shown in Fig. 9. Coefficient of lift and drag requirement are low during the beginning of the maneuver as the dynamic pressure is significant to generate desired aerodynamic forces. However, with the increase of altitude and velocity reduction, the coefficients spike to overcome the dynamic pressure deficiency. This particularly holds for the change from windward climb to tailwind descent turning phase. Unsteady aerodynamic effects are generally present for non-smooth temporal behavior of aerodynamic coefficients. In Fig. 9, overall behavior of aerodynamic coefficients is smooth in nature thereby suggesting minimum effect of unsteady phenomena. However, couple of minor kinks in the drag behavior are observed during the turning phase that may be assumed to have negligible effect. Therefore, the simulation results are adequate to suggest potential benefits of morphing during loiter mode of dynamic soaring maneuvers.
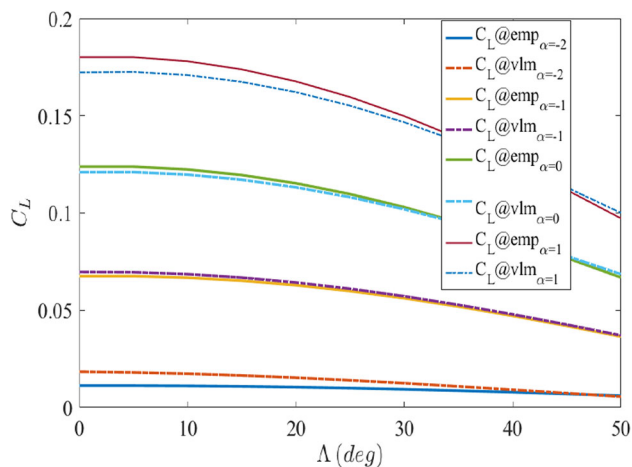
Comparison of aerodynamic coefficient (C_L) calculated through empirical technique was duly verified through vortex lattice method (VLM) methodology. Fig. 10 depicts variation in lift coefficient with respect to varying sweep angle for different angles of attack. Results from both the empirical and VLM methodologies are superimposed for analysis purpose. It is evident that both the methodologies follow a similar pattern, which shows the accuracy of the empirical technique utilized in this study for predicting the aerodynamic forces.

The objective of the trajectory optimization formulation is to reduce the overall wind shear requirement. It can be clearly seen from Fig. 11 that the minimum shear wind strength required for dynamic soaring maneuver with fixed configuration is 11.8 m/s and 9.8 m/s with morphing feature at an altitude of 10 m above ground level. The advantage increases with the increase in altitude suggesting morphing to be more effective at high altitudes. Reduction in the wind shear requirements is the fundamental challenge in executing dynamic soaring maneuvers. These results strongly support the utility of morphing to execute dynamic soaring maneuvers in low wind conditions typically found in urban areas. Operations such as area surveillance/ reconnaissance, medical support, search and rescue and various types of other missions are frequently required in such urban areas. In this study, the morphing configuration reduces minimum wind shear requirements by approximately 24% at different altitudes (10 m, 20 m and 30 m). This substantiates the fact that a morphing capable UAV could perform dynamic soaring in areas where wind shear is not of the magnitude that could support dynamic soaring for a fixed planform UAV.

Likewise, the normalized energies (total, potential and kinetic energies) are also higher in the case of morphing configuration (Fig. 12). Approximately, 34% increase in the total normalized energy is achieved by morphing UAV in comparison with the fixed-wing configuration. The kinetic energy is
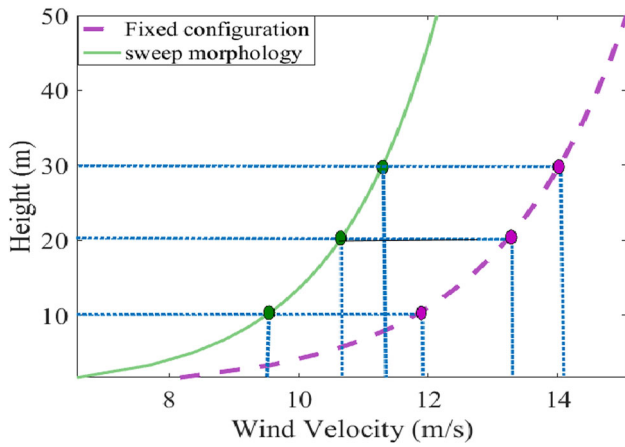
Fig. 11 Optimal trajectories for minimum required wind shear

exchanged for the potential energy as the UAV gains height. After reaching maximum altitude, the UAV takes the high altitude turn and start its downwind flight where the poten-

tial energy is traded for the kinetic energy. The overall energy at the start and end of the maneuver remains constant which ensures an energy neutral cycle.

The entire results of this section are summarized and collected in Table 2. In Table 2, all conducted comparisons between the sweep morphology and the fixed configuration are presented. It is noticeable that sweep morphology is better then fixed configuration in the results of achieving higher velocities, greater area coverage, higher altitude gains, lesser required minimum wind shear, low drag generations at low angles of attack (lower altitudes), and high lift generation at high angles of attack (higher altitude).

4 Conclusions

This paper proposed the idea of implementing dynamic soaring maneuver for a morphing capable platform. As a test case, impact of morphing was investigated for a platform capable

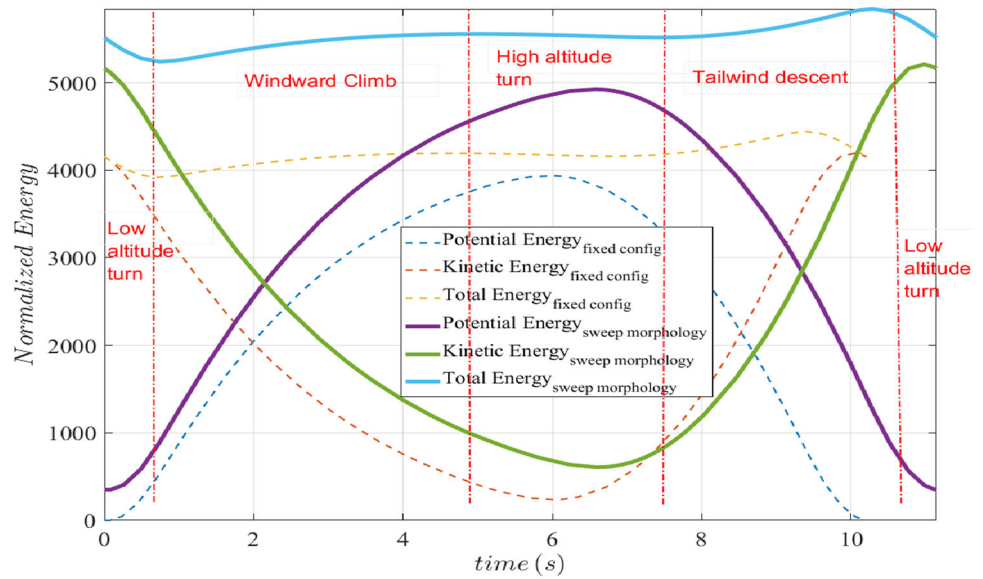**Fig. 12** Normalized energy during four different phases of the loiter maneuver

Table 2 Comparative analysis: Morphing vs. fixed configuration

No.	Nomenclature	Fixed configuration	Sweep Morphology (0°–50°)	% Improvement by morphing configuration w.r.t fixed configuration
1	Maximum altitude gain	37.5 m	48 m	29%
2	Distance covered in east direction	50 m	64 m	28%
3	Distance covered in north direction	17.5 m	22.25 m	25%
4	Maximum speed	27 m/s	30 m/s	13%
5	Normalized energy	4170	5540	34%
6	Maximum C_L requirement	0.45	0.39	10%
7	Minimum required wind shear (10 m)	11.8 m/s	9.5 m/s	24%
8	Maximum required angle of attack	4.5 °	3.9 °	16%
9	Max drag reduction	0.031	0.025	20%

of performing sweep variation (0°–50°) during the soaring maneuver. Utilizing nonlinear logarithmic wind shear model and a three-dimensional point-mass model, an optimal control problem was formulated and solved numerically utilizing Guass pseudospectral-based optimization solver GPOPS-II. Analysis revealed striking results as the morphing platform outclassed the fixed configuration platform in all aspects during the dynamic soaring loiter maneuver. Approximately, 24% lesser wind shear was required by the morphing platform in comparison to the fixed counterpart. This reflects that morphing platform could perform dynamic soaring in areas where fixed configurations might not possibly perform because of the presence of lesser wind shear. This will be of significant importance in applications where UAV is required to perform surveillance over urban areas where wind shear is lesser in magnitude due to surrounding interferences. Apart from this, the morphing platform showed approximately 29%, 28% and 25% improvement in the altitude, east and north distances, respectively. Also, considerable decrease in drag (20%) and lift requirement (10%) was demonstrated by the morphing platform. Approximately, 34% increased normalized energy and 13% increased velocity during the maneuver showed the effectiveness of the proposed integration. Through the results achieved, the idea of integrating dynamic soaring and morphology is highly supported. It is envisaged that this study will open a new avenue for researchers where the impact of various other morphologies (such as but not limited to wing twist, wing dihedral, span variation) on dynamic soaring heuristics can be analyzed to determine the configuration most suitable for dynamic soaring during different phases of the maneuver.

References

1. Maqsood A, Go TH (2010) Optimization of hover-to-cruise transition maneuver using variable-incidence wing. J Aircr 47(3):1060–1064
2. Maqsood A, Go TH (2012) Optimization of transition maneuvers through aerodynamic vectoring. Aerosp Sci Technol 23(1):363–371
3. AliKhan M, Peyada NK, Go TH (2013) Flight dynamics and optimization of three-dimensional perching maneuver. J Guid Control Dyn 36(6):1791–1797
4. Afonso F, Vale J, Lau F, Suleman A (2017) Performance based multidisciplinary design optimization of morphing aircraft. Aerosp Sci Technol 67:1–12
5. Wickenheiser AM, Garcia E (2008) Optimization of perching maneuvers through vehicle morphing. J Guid Control Dyn 31(4):815–823
6. Bye D, McClure P (2007) Design of a morphing. In: 48th AIAA/ASME/ASCE/AHS/ASC structures, structural dynamics, and materials conference, pp 1728
7. Secanell M, Suleman A, Gamboa P (2006) Design of a morphing airfoil using aerodynamic shape optimization. AIAA J 44(7):1550–1562
8. Akhtar N, Whidborne J, Cooke A (2012) Real-time optimal techniques for unmanned air vehicles fuel saving. Proc Inst Mech Eng, Part G: J Aerosp Eng 226(10):1315–1328
9. Gao X-Z, Hou Z-X, Guo Z, Fan R-F, Chen X-Q (2014) Analysis and design of guidance-strategy for dynamic soaring with UAVs. Control Eng Pr 32:218–226
10. Gao X-Z, Hou Z-X, Guo Z, Chen X-Q (2015) Energy extraction from wind shear: reviews of dynamic soaring. Proc Inst Mech Eng, Part G: J Aerosp Eng 229(12):2336–2348
11. Liu D-N, Hou Z-X, Guo Z, Yang X-X, Gao X-Z (2017) Bio-inspired energy-harvesting mechanisms and patterns of dynamic soaring. Bioinspiration Biomim 12(1):016014
12. Rayleigh L (1883) The soaring of birds. Nature 27(701):534–535
13. Alerstam T, Gudmundsson GA, Larsson B (1993) Flight tracks and speeds of Antarctic and Atlantic seabirds: radar and optical measurements. Philos Trans R Soc Lond B 340(1291):55–67
14. Weimerskirch H, Bonadonna F, Bailleul F, Mabille G, Dell'Omo G, Lipp H-P (2002) GPS tracking of foraging albatrosses. Science 295(5558):1259–1259
15. Ariff O, Go T (2011) Waypoint navigation of small-scale UAV incorporating dynamic soaring. J Navig 64(1):29–44
16. Sachs G, da Costa O (2003) Optimization of dynamic soaring at ridges. In: AIAA Atmospheric flight mechanics conference and exhibit, pp 11–14
17. Idrac P (1932) Experimentelle Untersuchungen über den Segelflug, na
18. Sachs G (2005) Minimum shear wind strength required for dynamic soaring of albatrosses. Ibis 147(1):1–10
19. Gordon RJ (2006) Optimal dynamic soaring for full size sailplanes, Tech. report. Air Force Inst of Tech Wright-Patterson AFB OH Dept of Aeronautics and Astronautics
20. Zhao YJ (2004) Optimal patterns of glider dynamic soaring. Optim Control Appl Methods 25(2):67–89
21. Zhao YJ, Qi YC (2004) Minimum fuel powered dynamic soaring of unmanned aerial vehicles utilizing wind gradients. Optim Control Appl Methods 25(5):211–233
22. Liu D-N, Hou Z-X, Gao X-Z (2017) Flight modeling and simulation for dynamic soaring with small unmanned air vehicles. Proc Inst Mech Eng, Part G: J Aerosp Eng 231(4):589–605
23. Mir I, Maqsood A, Akhtar S (2017) Optimization of dynamic soaring maneuvers for a morphing capable UAV. AIAA Information Systems-AIAA Infotech@ Aerospace, pp 0678
24. Mir I, Maqsood A, Akhtar S (2017) Optimization of dynamic soaring maneuvers to enhance endurance of a versatile UAV. Mater Sci Eng Conf Ser 211:012010
25. Bonnin V, Bénard E, Moschetta J-M, Toomer C (2015) Energy-harvesting mechanisms for UAV flight by dynamic soaring. Int J Micro Air Veh 7(3):213–229
26. Lentink D, Müller U, Stamhuis E, De Kat R, Van Gestel W, Veldhuis L, Henningsson P, Hedenström A, Videler JJ, Van Leeuwen JL (2007) How swifts control their glide performance with morphing wings. Nature 446(7139):1082
27. Barnes JP (2004) How flies the albatross-the flight mechanics of dynamic soaring. Tech. Report, SAE Technical Paper
28. Jha AK, Kudva JN (2004) Morphing aircraft concepts, classifications, and challenges, smart structures and materials 2004: industrial and commercial applications of smart structures technologies, vol 5388, International Society for Optics and Photonics, pp 213–225
29. Dayyani I, Shaw A, Flores ES, Friswell M (2015) The mechanics of composite corrugated structures: A review with applications in morphing aircraft. Compos Struct 133:358–380
30. Ajaj RM, Jankee GK (2018) The transformer aircraft: a multimission unmanned aerial vehicle capable of symmetric and asymmetric span morphing. Aerosp Sci Technol 76:512–522

31. Gandhi UN, Nam T (2017) Shape morphing fuselage for an aerocar, Feb. 7 2017, US Patent 9,561,698

32. Oktay T, Coban S (2017) Lateral autonomous performance maximization of tactical unmanned aerial vehicles by integrated passive and active morphing. Int J Adv Res Eng 3(1):1–5

33. Chinnapathlolla AR, Krishnamurthy RB, Rogers D (2015) Trigger based portable device morphing, June 25 2015, US Patent App. 14/138,728

34. Barbarino S, Bilgen O, Ajaj RM, Friswell MI, Inman DJ (2011) A review of morphing aircraft. J Intell Mater Syst Struct 22(9):823–877

35. Blondeau J, Richeson J, Pines D (2003) Design of a morphing aspect ratio wing using an inflatable telescoping spar. In: 44th AIAA/ASME/ASCE/AHS/ASC Structures, structural dynamics, and materials conference, pp 1718

36. Prabhakar N, Prazenica RJ, Gudmundsson S (2015) Dynamic analysis of a variable-span, variable-sweep morphing UAV. In: Aerospace conference, 2015 IEEE, IEEE, pp 1–12

37. Kendall GT, Lisoski DL, Morgan WR, Griecci, JA (2017) Active dihedral control system for a torsionally flexible wing, Sept. 19 2017, US Patent 9,764,819

38. Weisshaar TA (2013) Morphing aircraft systems: historical perspectives and future challenges. J Aircr 50(2):337–353

39. Roth B, Crossley W (2003) Application of optimization techniques in the conceptual design of morphing aircraft. In: AIAA's 3rd Annual aviation technology, integration, and operations (ATIO) forum, pp 6733

40. Schmidt LV (1998) Introduction to aircraft flight dynamics, 1st edn. American Institute of Aeronautics and Astronautics, Inc., Reston

41. Peters Jr. SE (2000) Aircraft structure to improve directional stability, Aug. 8 2000, US Patent 6,098,923

42. Anglin EL, Chambers J (1969) Analysis of lateral directional stability characteristics of a twin jet fighter airplane at high angles of attack. Nasa Technical Note, NASA TN D-5361, Nasa

43. Phillips WH (1948) Effect of steady rolling on longitudinal and directional stability. Nasa Technical Note, NASA TN 1627, Nasa

44. Abzug MJ, Larrabee EE (2005) Airplane stability and control: a history of the technologies that made aviation possible, vol 14. Cambridge University Press, Cambridge

45. Patterson MA, Rao AV (2014) GPOPS-II: A MATLAB software for solving multiple-phase optimal control problems using hp-adaptive Gaussian quadrature collocation methods and sparse nonlinear programming. ACM Trans Math Softw (TOMS) 41(1):1

46. Wharington JM (2004) Heuristic control of dynamic soaring, Control Conference, 2004. 5th Asian IEEE, vol 2, pp 714–722

47. Anderson JD (1999) Aircraft performance and design. McGraw-Hill Science/Engineering/Math, Maidenheach

48. Mir I, Taha H, Eisa SA, Maqsood A (2018) A controllability perspective of dynamic soaring. Nonlinear Dyn 93:1–16

49. Patterson MA, Rao AV (2013) GPOPS-II version 1.0: a general-purpose MATLAB toolbox for solving optimal control problems using the Radau pseudospectral method. University of Florida, Gainesville, pp 32611–6250

50. Patterson MA, Hager WW, Rao AV (2015) A pH mesh refinement method for optimal control. Optim Control Appl Methods 36(4):398–421

51. Zhao P, Mohan S, Vasudevan R (2017) Optimal control for nonlinear hybrid systems via convex relaxations. arXiv:1702.04310 (**preprint**)

52. Liu F, Hager WW, Rao AV (2018) Adaptive mesh refinement method for optimal control using decay rates of Legendre polynomial coefficients. IEEE Trans Control Syst Technol 26(4):1475–1483

53. Kelly M (2017) An introduction to trajectory optimization: how to do your own direct collocation. SIAM Rev 59(4):849–904